UHF-RFID Backscatter Channel Analysis for Accurate Wideband Ranging

Stefan Hinteregger*, Josef Kulmer*, Michael Goller†, Florian Galler‡, Holger Arthaber‡, Klaus Witrisal*
*Graz University of Technology, †Detego GmbH, ‡Vienna University of Technology, Austria
email: stefan.hinteregger@tugraz.at

***Abstract*—Positioning and ranging within UHF RFID are highly dependent on the channel characteristics. The accuracy of time-of-flight based ranging systems is fundamentally limited by the available bandwidth. This paper first analyzes the UHF RFID backscatter channel formed by convolution of the individual constituent channels. For this purpose, we present comprehensive wideband channel measurements in two representative scenarios and an analysis with respect to the Rician K-factor for the line-of-sight component, the root-mean-square delay spread, and the coherence distance, which all influence the potential positioning performance.**

Based on these measurements, we validate the Cramér Rao lower bound for time-of-flight based ranging under the influence of dense multipath and present two types of range estimators, a maximum likelihood and a matched filter approach. The resulting range estimates highlight the need for an increased bandwidth for UHF RFID systems with respect to time-of-flight based ranging.

I. Introduction

Accurate and robust ranging and positioning with ultra-high frequency (UHF) radio frequency identification (RFID) tags is a key-enabler for a variety of applications in production, supply chain management, and retail. Many of these application scenarios require a sub-meter accuracy, which is still an unsolved challenge. For time-of-flight based ranging systems, the available bandwidth imposes a fundamental limit to the achievable accuracy.

A thorough characterization of the UHF RFID channel is necessary for developing robust ranging algorithms. For narrowband signals, the backscatter (BS) channel has been well analyzed with respect to fading statistics [1]. Several measurement campaigns [1]–[5] have studied the individual (*i.e.* up- and downlink) channels in both the narrowband and the wideband regimes, but only some analyses of wideband parameters like the Rician K-factor for the LOS component or the root-mean-square (rms) delay spread have been performed [2].

The application driven requirement of sub-meter ranging and positioning leads to a clear trend towards larger bandwidth systems in the UHF-RFID technology [6]–[8]. Ranging methods are heavily influenced by the wideband statistics of the BS channel. The achievable ranging performance has been analyzed for different scenarios. E.g. in ultra-wideband settings the Cramér Rao lower bound [9] and the Ziv-Zakai bound [10] have been derived. The Cramér Rao lower bound in dense multipath channels [11] has been extensively studied with respect to positioning applications and has been applied to a wideband UHF-RFID scenario [8].

Channel knowledge is not only important for localization but also for system performance simulations. The channel model used and analyzed in this paper could be applied to RFID software simulators like [12], [13] with different levels of adaptation. The inclusion of the channel model in the network simulators ns-2 and ns-3 is more difficult since the focus of these simulators is on multiple access and routing protocols and usually no signal-level simulation is performed [14].

Taking into account the requirements and the current state of the research, the main contributions of this paper are two-fold: First, we analyze comprehensive channel measurements from two scenarios in the UHF-RFID frequency range with a focus on the wideband channel parameters. Second, we analyze and validate the ranging error bound for dense multipath channels using the channel measurement data and two time-of-flight estimation approaches.

II. Problem Formulation

We investigate the BS channel between an RFID reader antenna ℓ at known position $\mathbf{p}_\ell$, a tag at unknown position $\mathbf{p}$ which scatters back the received signal, and another RFID reader antenna ℓ' at known position $\mathbf{p}_{\ell'}$. Each of the L RFID reader antennas can be used to transmit and/or receive a wideband signal [6], [8]. The aim is to find the overall propagation delay of the BS channel which is proportional to the time-of-flight between the transmitting RFID reader antenna via the tag to the receiving RFID reader antenna.

A. Channel Model

The BS channel can be described by the convolution of the individual downlink and the uplink channels (cf. Fig. 1a). The channel impulse responses (CIR) of these individual channels are modeled by a line-of-sight (LOS) plus dense multipath (DM) model [11]

$$h_\ell(\tau) = \alpha_\ell \delta(\tau - \tau_\ell) + \nu_\ell(\tau). \tag{1}$$

The LOS is characterized by its complex-valued amplitude α_ℓ and delay $\tau_\ell = \frac{1}{c}\|\mathbf{p}_\ell - \mathbf{p}\|$ equivalent to the Euclidean distance between the reader's and tag's positions scaled by the speed of light c, where $\delta(\tau)$ is the Dirac pulse. The term $\nu_\ell(\tau)$ in (1)

This work was performed within the project REFlex, funded by the Austrian Research Promotion Agency (FFG; project number: 845630).

models the dense multipath (DM) consisting of all occurring multipath components (MPC), including reflections at flat surfaces and scattering at small objects. This DM is modeled as a zero-mean complex Gaussian random process, assuming uncorrelated scattering [15] along the delay axis τ. Thus, the auto-correlation function of the DM is $\mathbb{E}\{\nu_\ell(\tau)[\nu_\ell(u)]^*\} = S_{\nu,\ell}(\tau)\delta(\tau-u)$ with $S_{\nu,\ell}(\tau)$ as the power-delay-profile (PDP) of the DM which is zero for $\tau < \tau_\ell$. We also assume quasi-stationarity in the spatial domain, meaning that for one reader / tag configuration, the PDP does not change noticeably in the vicinity of the tag [16]. The signal model does not include more than one tag. This does not limit the system operation to one tag, but rather implies the usage of multiple access schemes [6], [7] to separate multiple tags.

To analyze the overall BS channel, the convolution of the downlink from reader antenna ℓ to the tag and the uplink from the tag to reader antenna ℓ' can be written as another LOS plus DM model

$$\begin{aligned} h_{\ell,\ell'}(\tau) &= (h_\ell * h_{\ell'})(\tau) \\ &= \alpha_\ell\alpha_{\ell'}\delta(\tau-\tau_\ell-\tau_{\ell'}) + \nu_{\ell,\ell'}(\tau). \end{aligned} \tag{2}$$

We can model $\nu_{\ell,\ell'}(\tau)$ by a PDP [2]

$$\begin{aligned} S_{\nu,\ell,\ell'}(\tau) = (1+\kappa)\big[&|\alpha_{\ell'}|^2 S_{\nu,\ell}(\tau-\tau_{\ell'}) \\ &+|\alpha_\ell|^2 S_{\nu,\ell'}(\tau-\tau_\ell) + (S_{\nu,\ell} * S_{\nu,\ell'})(\tau)\big] \end{aligned} \tag{3}$$

where κ describes the correlation of the down and uplink channels and is between 0 and 1 for uncorrelated and fully-correlated constituent channels, respectively. This means that the power in the DM is doubled with respect to the LOS component for fully-correlated channels [2].

B. Received Signal

The received signal[1] $r(t)$ results as convolution of a transmitted baseband signal $s(t)$ and the overall BS channel described in (2) as

$$r(t) = \alpha_\ell\alpha_{\ell'}s(t-\tau_\ell-\tau_{\ell'}) + (s*\nu_{\ell,\ell'})(t) + \omega(t) \tag{4}$$

where $\omega(t)$ is additive white Gaussian noise (AWGN) with a two-sided power spectral density of $N_0/2$.

C. Range Estimation

The distance between the transmit reader, the tag, and the receive reader is given by $d_{\text{BS}} = c(\tau_\ell + \tau_{\ell'})$. For easier readability the following abbreviations will be used: $\alpha_{\text{BS}} = \alpha_\ell\alpha_{\ell'}$, and $\tau_{\text{BS}} = \tau_\ell + \tau_{\ell'}$. By sampling the received signal with $f_{\text{s}} = 1/T_{\text{s}}$, with T_{s} as sampling period, (4) can be written in vector notation as

$$\mathbf{r} = \alpha_{\text{BS}}\mathbf{s}_{\tau_{\text{BS}}} + \mathbf{n}_{\text{c}} + \boldsymbol{\omega} \tag{5}$$

[1]This model assumes perfect (frequency independent) backscattering of the tag over the whole bandwidth. This certainly does not hold when considering 'wideband' signals, but the smaller the bandwidth gets, the less frequency dependent the radar cross section of a tag gets [17]. It would be possible to include the frequency dependent behavior in the baseband pulse $s(t)$ [18], but in this work we want to focus on the influence of the channels, and thus neglect this effect.

where $\mathbf{s}_{\tau_{\text{BS}}} = [s(-\tau_{\text{BS}}), s(T_{\text{s}}-\tau_{\text{BS}}),\ \dots, s((N-1)T_{\text{s}}-\tau_{\text{BS}})]^T$, $\mathbf{n}_{\text{c}} = [(s*\nu_{\ell,\ell'})(0), (s*\nu_{\ell,\ell'})(T_{\text{s}}),\ \dots, (s*\nu_{\ell,\ell'})((N-1)T_{\text{s}})]^T$, and $\mathbf{r}$ and $\boldsymbol{\omega}$ are sampled versions of the received signal and the AWGN as vectors $\in \mathbb{R}^{N\times 1}$, long enough to include all MPCs.

Using the Gaussian assumption, the likelihood function of the received signal, parametrized by the unknown parameter vector $\boldsymbol{\theta} = [\tau_{\text{BS}}, \mathcal{R}\{\alpha_{\text{BS}}\}, \mathcal{I}\{\alpha_{\text{BS}}\}]^T$, is

$$f(\mathbf{r};\boldsymbol{\theta}) \propto \exp\{(\mathbf{r}-\alpha_{\text{BS}}\mathbf{s}_{\tau_{\text{BS}}})^H\mathbf{C}^{-1}(\mathbf{r}-\alpha_{\text{BS}}\mathbf{s}_{\tau_{\text{BS}}})\}, \tag{6}$$

where $\mathbf{C} = \mathbf{S}^H\mathbf{S}_{\boldsymbol{\nu},\ell,\ell'}\mathbf{S} + \frac{N_0}{T_{\text{s}}}\mathbf{I} \in \mathbb{R}^{N\times N}$ is the covariance matrix with $\mathbf{S} = [\mathbf{s}_0,\ \dots, \mathbf{s}_{(N-1)T_{\text{s}}}]^T$ and $\mathbf{S}_{\boldsymbol{\nu},\ell,\ell'} = \text{diag}\{S_{\nu,\ell,\ell'}(iT_{\text{s}})\cdot T_{\text{s}}\}$ is a diagonal matrix containing the PDP.

To estimate the distance d_{BS}, we apply: (i) a maximum likelihood (ML) estimator, and (ii) a naïve matched filter (MF) estimator. The ML estimator accounts for the influence of the DM expressed by the covariance matrix and thus requires the PDP of the DM and N_0 to be known. The ML estimator is found by maximizing the likelihood function (6) with respect to the parameters τ_{BS} and α_{BS}. The nuisance parameter α_{BS} has to be estimated jointly with τ_{BS} [19], which can be written as

$$\hat{\alpha}_{\text{BS}}(\tau_{\text{BS}}) = \frac{\mathbf{r}^H\mathbf{C}^{-1}\mathbf{s}_{\tau_{\text{BS}}}}{\mathbf{s}_{\tau_{\text{BS}}}^H\mathbf{C}^{-1}\mathbf{s}_{\tau_{\text{BS}}}}. \tag{7}$$

The ML estimator is now solely depending on τ_{BS} and can be written as

$$\hat{d}_{\text{BS,ML}} = c\cdot\underset{\tau_{\text{BS}}}{\text{argmax}}\{f(\mathbf{r};\boldsymbol{\theta})\} \quad \text{subject to (7).} \tag{8}$$

The MF estimator simply correlates the received signal with the transmit pulse and searches for the maximum, i.e.

$$\hat{d}_{\text{BS,MF}} = c\cdot\underset{\tau_{\text{BS}}}{\text{argmax}}\{\mathbf{r}^H\mathbf{s}_{\tau_{\text{BS}}}\}. \tag{9}$$

This estimator ($\hat{d}_{\text{BS,MF}}$) would be optimal for a signal model without the DM [19, p. 192].

D. Ranging Error Bound $\mathcal{R}(\tau)$

The Cramér Rao lower bound for the delay estimation problem for DM channels [11], called ranging error bound (REB), is given by the inverse of the square root of the equivalent Fisher information (EFI) for the delay estimation problem,

$$\mathcal{R}(\tau_{\text{BS}}) = \sqrt{\mathcal{I}_{\tau_{\text{BS}}}^{-1}}. \tag{10}$$

For a BS channel the EFI is $\mathcal{I}_{\tau_{\text{BS}}} = 8\pi^2\beta^2\widetilde{\text{SINR}}_{\text{BS}}$, where $\beta^2 = \|\dot{\mathbf{s}}_{\tau_{\text{BS}}}\|/(4\pi^2\|\mathbf{s}_{\tau_{\text{BS}}}\|)$ is the effective (mean-square) bandwidth of the transmit pulse, $\dot{\mathbf{s}}_{\tau_{\text{BS}}}$ is the derivative of $s(t-\tau_{\text{BS}})$ with respect to t, and $\widetilde{\text{SINR}}_{\text{BS}}$ is the effective signal-to-interference-plus-noise-ratio (SINR) [8]. In particular, the effective SINR describes the useful ranging information of the LOS component when influenced by DM and AWGN and can be factored into three parameters [11]:

(i) the SINR which quantifies the signal-to-noise-ratio (SNR) after the square root of the covariance matrix has been applied as whitening filter,

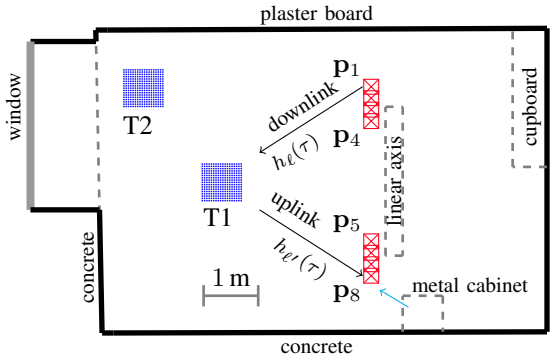

(a) Scenario A: A laboratory at Vienna University of Technology with some furniture and a linear axis. Eight closely-spaced Vivaldi antennas arranged as two arrays ($\mathbf{p}_1$ to $\mathbf{p}_4$ & $\mathbf{p}_5$ to $\mathbf{p}_8$) and two different table positions (T1 & T2).

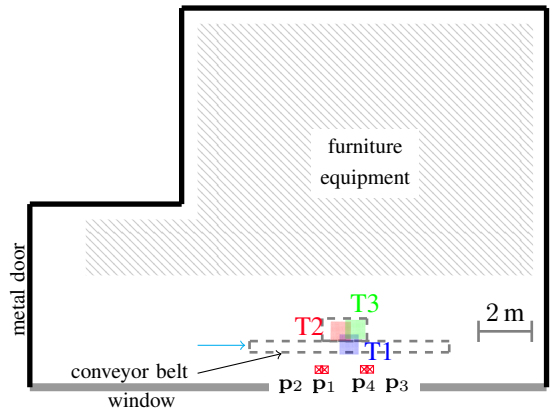

(b) Scenario B: Industrial setup with a conveyor belt, aluminum profiles, and many scatterers. Four closely-spaced Vivaldi antennas arranged as two arrays ($\mathbf{p}_1$ and $\mathbf{p}_2$ & $\mathbf{p}_3$ and $\mathbf{p}_4$) and three different table positions (T1, T2 & T3).

Fig. 1. Floorplans of the two measurement scenarios. At each table position, 306 measurements are obtained with a spacing of 4 cm on a 17×18 grid. The cyan arrows depict the point of views of the photographs presented in Fig. 2.

(ii) the whitening gain $\gamma = \frac{\dot{\mathbf{s}}_{\tau_{\mathrm{BS}}}^H \mathbf{C}^{-1} \dot{\mathbf{s}}_{\tau_{\mathrm{BS}}}}{\dot{\mathbf{s}}_{\tau_{\mathrm{BS}}}^H \mathbf{C}^{-1} \mathbf{s}_{\tau_{\mathrm{BS}}}} \frac{1}{4\pi^2\beta^2}$ which quantifies the gain due to the knowledge of the PDP,

(iii) and $\sin^2(\varphi)$ which is an information loss due to the estimation of the nuisance parameter α_{BS}.[2]

In Section V we validate the error bound $\mathcal{R}(\tau)$ described above using measurement data from two representative scenarios with the described maximum likelihood and matched filter estimators in order to show the practical applicability and to verify the modeling assumptions. Next, the measurement scenarios are described and basic channel parameters are analyzed.

III. Measurement Setup

The measurement data used in this work are obtained from a series of wideband measurements using an m-sequence channel sounder by Ilmsens [20] which operates in the frequency range (-10 dB cut-off) from 0.1 to 3.2 GHz. It has

[2] φ describes the angle between the whitened pulse and the whitened pulse derivative. For common pulses and an AWGN model, $\varphi = 90°$. Due to the whitening this angle gets smaller than 90°.

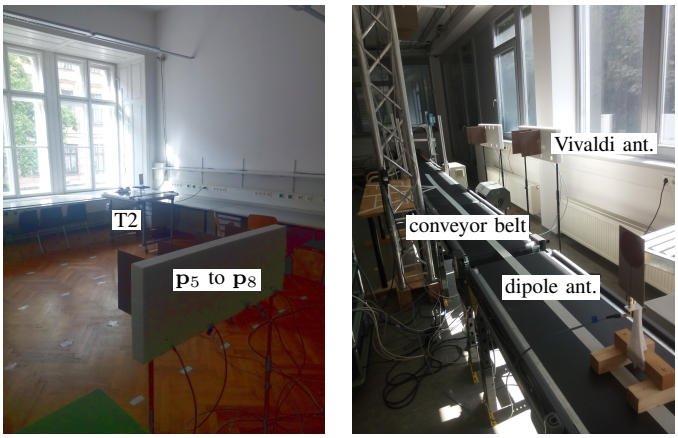

(a) Scenario A (b) Scenario B

Fig. 2. Pictures of the two measurement scenarios. The point of view with respect to the floorplan is shown as cyan arrow in Fig. 1.

one transmitting (TX) and two receiving channels (RX), a sampling frequency of 6.95 GHz, thus a resolution of 4.31 cm, and a maximum delay of 589.2 ns or 176.6 m corresponding to a sequence length of 4095. To measure up to four antennas per RX channel we use two RF switching matrices [21]. The cross-talk and the system-response of the measurement equipment are removed up to the antenna ports by a match-through calibration. This setup provides the flexibility to study different bi-static configurations, including single-input, single-output (SISO) as well as multiple-input, multiple-output (MIMO) setups to investigate the effects of diversity gain for the ranging / positioning problem.

A tapered slot antenna (also called Vivaldi antenna) with a 3-dB mainlobe width of approximately 90° is used as reader antenna. Its wideband gain pattern is not completely independent of frequency but shows good properties in the frequency range from 0.75 to 1.5 GHz. The tag antenna is an elliptic dipole-like structure with an omnidirectional gain pattern similar to RFID tags. Again, the wideband pattern shows good properties in the same frequency range as the reader antennas.

A positioning table is used to accurately position the RFID tag in an automated way to obtain a large number of measurements with different tag positions. The positioning table spans a 0.68×0.64 m grid with a spacing of 4 cm. For the individual measurement runs, the positioning table can be placed at different locations in the room in order to evaluate the desired coverage.

Measurement data have been acquired in two different scenarios: Scenario A is a standard laboratory hall at Vienna University of Technology that was chosen in order to evaluate a typical indoor lab / office environment. In contrast, Scenario B is an industrial hall with a significant amount of metal fixtures. Both scenarios are described in more detail in the following sections.

A. Scenario A

In Fig. 1a and Fig. 2a the floorplan and a picture of the measurement scenario in the laboratory are depicted, respectively. The positioning table with the tag antenna is placed at two positions in the room (T1 & T2), while the reader antennas are set up as two linear arrays with antenna positions at $\mathbf{p}_1$ to $\mathbf{p}_4$ & $\mathbf{p}_5$ to $\mathbf{p}_8$. The back of the room holds a cupboard with laboratory equipment, while the other side of the room is occupied by a metal cabinet. Furthermore, the lab holds a set of aluminum profiles for linear axis movements that is placed directly behind the antennas. All antennas are set up at a constant height of 1.3 m.

B. Scenario B

The second measurement campaign (see floorplan in Fig. 1b and picture in Fig. 2b) has been performed in an industrial hall with metal fixtures and a conveyor belt setup as typically found in manufacturing and logistics. The hall is approximately 18 by 12 m large and the facilities are used to analyze and study logistic processes and systems, e.g. for consignment / picking of goods. The positioning table is placed at three partly overlapping positions (T1, T2, T3) in three consecutive measurement runs and two readers, each having two antennas (at $\mathbf{p}_1$, $\mathbf{p}_2$ & $\mathbf{p}_3$, $\mathbf{p}_4$), are emulated. All antennas are set up at a constant height of 1.3 m.

C. Pre-processing

The measurement setup in the two described scenarios includes a data processing pipeline comprising the following steps: First, the cross-talk and system-response are removed to find calibrated downlink and uplink channel measurements. These measurements are subsequently convolved with each other to get calibrated measurements of the BS channel. Next, this BS signal is converted to baseband using a center frequency of $f_c = 900$ MHz. Finally, the bandwidth is reduced by convolution with a root-raised-cosine pulse with a pulse duration of $T_p = 1$ ns and roll-off-factor of 0.6 which acts as baseband pulse $s(t)$. The result of this pre-processing is called channel response (CR) $\mathbf{g}_{\text{BS}}$ given by

$$\mathbf{g}_{\text{BS}} = \alpha_{\text{BS}}\mathbf{s}_{\tau_{\text{BS}}} + \mathbf{n}_c. \tag{11}$$

In contrast to the received signal model, the actual signal contains AWGN which is neglected in further considerations due to the high SNR of the employed channel sounder.

Due to the large bandwidth, we can assume that the LOS can be resolved from the multipath components which enables us to estimate α_{BS} by a projection $\hat{\alpha}_{\text{BS}} = \mathbf{g}_{\text{BS}}^H \mathbf{s}_{\tau_{\text{BS,GM}}} T_s$ of the CR onto the baseband pulse at the true delay given by the geometric model $\tau_{\text{BS,GM}} = \frac{1}{c}(\|\mathbf{p}_\ell - \mathbf{p}\| + \|\mathbf{p} - \mathbf{p}_{\ell'}\|)$. This estimate is used for the following channel analysis.

IV. Channel Analysis

In order to investigate the properties of the BS channel with a focus on ranging and positioning, we consider the following three parameters for the analysis:

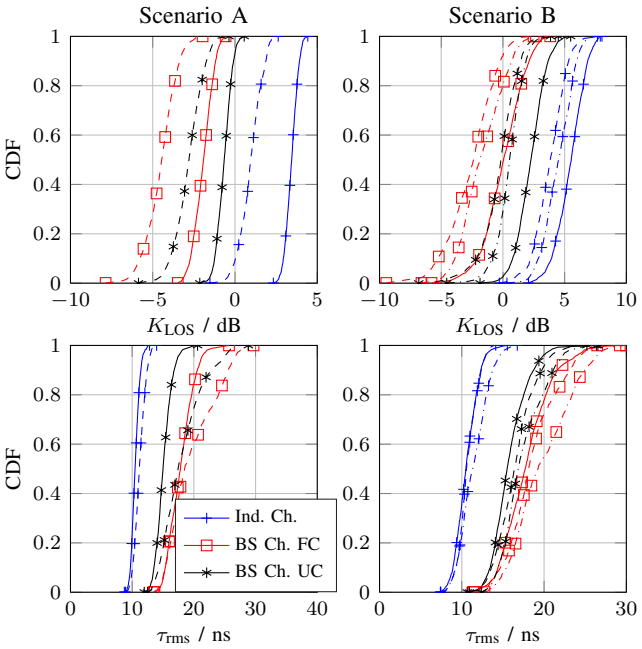

Fig. 3. Cumulative Distribution Functions of the two parameters (1st row K_{LOS}, 2nd row τ_{rms}) for both individual (Ind.) and backscatter (BS) channels for for Scenario A (left column) and Scenario B (right column). The different line types distinguish the different table positions (solid lines: T1, dashed lines: T2, dash-dotted lines: T3). Additionally the BS channels are separated into fully correlated (FC) and uncorrelated channels (UC).

a) Rician K-factor for the LOS component: The ranging performance is highly influenced by the power ratio between the LOS component and all NLOS components [22]. This power ratio is comparable to the Rician K-factor in narrowband systems and is termed Rician K-factor for the LOS component K_{LOS}. Instantaneous K_{LOS} values are computed from individual CRs by

$$\hat{K}_{\text{LOS}} = \frac{\|\hat{\alpha}_{\text{BS}}\mathbf{s}_{\tau_{\text{BS,GM}}}\|^2}{\|\mathbf{g}_{\text{BS}} - \hat{\alpha}_{\text{BS}}\mathbf{s}_{\tau_{\text{BS,GM}}}\|^2} \tag{12}$$

b) Root-mean-square delay spread τ_{rms}: The root-mean-square delay spread quantifies the arrival times of MPCs with significant energy and is estimated from the second centralized moment of instantaneous normalized PDPs including the LOS component, i.e. $|\mathbf{g}_{\text{BS}}|^2$.

c) Spaced-distance-correlation-function: For methods using the spatial domain (e.g. beamforming, combining of measurements from closely-spaced antennas) uncorrelated measurements are usually preferred to get additional information [8]. We analyze the spaced-distance-correlation-function (SDCF) of the DM which expresses the percentage of correlation at a certain distance. To compute the SDCF for a specific BS channel and a specific grid point $\mathbf{p}_c$, we find all points on the grid with a certain distance (e.g. 16 ± 2 cm), $\mathcal{P}_c = \{\mathbf{p}_i : \|\mathbf{p}_i - \mathbf{p}_c\| = 16 \pm 2\,\text{cm}\}$, shift the CRs along time domain such that the LOS delay coincides with the LOS of the center point $\mathbf{p}_c$, estimate the mean of the complex channel coefficients for the LOS component, subsequently subtract the LOS component, compute the correlation coefficients between

the channel transfer functions of the DM at $\mathbf{p}_\mathrm{c}$ with all $\mathbf{p}_i$, and average over all points in $\mathcal{P}_c$.

For the two scenarios described in Section III, we evaluate the described parameters, for all individual channels and all BS channels, and discuss the results and their implications for the ranging problem.

A. Analysis for Scenario A

The channel-analysis results are shown in Fig. 3 as cumulative distribution functions (CDF). The left column is for Scenario A. Solid and dashed lines are table positions T1 and T2 respectively. The BS channel results, which are separated in fully correlated (FC - red and squares) channels (downlink =uplink / $\ell = \ell'$) and (partly) uncorrelated (UC - black and asterisks) channels ($\ell \neq \ell'$), and the individual (Ind. - blue and crosses) channel (downlinks/uplinks) results are depicted.

The K_LOS factor (in dB) for the individual channels is always positive for T1 (median of $4.2\,$dB), while for T2 it is positive for $80\,\%$ of the measurements (median of $0.9\,$dB). This reduction is explained by the larger distance to T2 since the power in the LOS component decreases faster than the power in the NLOS components. According to theory [2] the Rician K-factor for the LOS component of a BS channel is

$$K_{\mathrm{LOS},\ell,\ell'} = \left(1 - \frac{\kappa}{2}\right) \frac{K_{\mathrm{LOS},\ell} K_{\mathrm{LOS},\ell'}}{1 + K_{\mathrm{LOS},\ell} + K_{\mathrm{LOS},\ell'}}. \qquad (13)$$

Equ. (13) shows that the backscatter K_LOS factor is dominated by the smaller of the two individual factors and that for fully correlated individual channels, a $3\,$dB loss is expected compared to uncorrelated channels. In Fig. 3, this loss is only $2\,$dB because the assumption of fully uncorrelated channels does not hold true within this set-up.

The rms delay spread for the individual channels is slightly larger for T2 explained by the same reasoning as above, that the LOS component attenuates faster with increasing distance than the NLOS components. The rms delay spread is larger for the BS channels since the delays are extended by the convolution of the channels (cf. (3)). The FC data have a larger rms delay spread than the UC data because the power in the NLOS component is increased up to a factor of two.

The median of the SDCF evaluated at a spacing of $16\,$cm is 0.7 for both individual and the uncorrelated BS channels, and below 0.4 to 0.5 for the BS channels. With increasing distance (cmp. T1 and T2) the correlation of the DM is slightly reduced for both the individual and the BS channels by a value of approximately 0.1.

B. Analysis for Scenario B

In the right column of Fig. 3, the CDFs are shown for the individual and BS channels for the measurements in the industrial hall for the three different table positions. The results compare well to the data gathered in the laboratory. The K_LOS factor for individual channels again exceeds $0\,$dB (median of $5\,$dB) and the results for the BS channel are slightly above the K_LOS factor obtained in the laboratory due to the shorter distances. The median of the rms delay spread is $17\,$ns for the BS and $11\,$ns for the individual channels. The median of the SDCF evaluated at $16\,$cm is 0.4 for the BS and 0.5 for the individual channels. The results for the different table positions are in general more homogeneous than for the laboratory scenario, since the table positions are partly overlapping.

V. Validation of the REB

We finally validate the REB presented in Sec. II-D with the measured data presented in Sec. IV over a wide bandwidth range and compare the results to simulated data.

A. Covariance Estimation

The maximum likelihood ranging estimator introduced in Sec. II-C requires the inverse of the covariance matrix of DM plus AWGN. The covariance matrix is determined as follows[3]. At each table position, the overall 18×17 grid is reduced to smaller subgrids (7×7), leading to $N_\mathrm{sg} = 132$ partly overlapping subgrids. This reduction of the grid is necessary since the covariance matrix of DM is position dependent. The following processing steps are conducted:

- Extract channel responses $\mathbf{g}_{\mathrm{BS},1\,\mathrm{GHz}}$ at the largest possible bandwidth ($1\,$GHz) on a subgrid.
- Align the channel responses such that the LOS components arrive at the same time τ_BS.
- Estimate the complex channel coefficients $\hat{\alpha}_\mathrm{BS}$ with the projection of the CR onto the baseband pulse $\mathbf{s}_{\tau_\mathrm{BS}}$.
- Compute the mean value of the estimated complex channel coefficients $\bar{\hat{\alpha}}_\mathrm{BS}$.
- At the target bandwidth, extract channel responses $\mathbf{g}_\mathrm{BS}$, align the signals such that the LOS components arrive at the same time, subtract the LOS signal $\bar{\hat{\alpha}}_\mathrm{BS}\mathbf{s}_{\tau_\mathrm{BS}}$ and compute the covariance matrix of the resulting signals.
- To arrive at the covariance matrix for DM plus AWGN we need to add N_0/T_s to the main diagonal. We find N_0 via the energy of the LOS component $E_\mathrm{LOS} = |\bar{\hat{\alpha}}_\mathrm{BS}|^2 \|\mathbf{s}_{\tau_\mathrm{BS}}\|^2 T_\mathrm{s}$. The SNR for the LOS component is set to $E_\mathrm{LOS}/N_0 = 25\,$dB for the following validation.

The resulting covariance matrix estimate is shown in Fig. 4 for a BW of $100\,$MHz. For the plot, the signals are shifted such that the LOS components arrive at $0\,$ns. The resulting estimate shows that the US assumption does not hold for the considered scenario. The off-diagonal terms stem from deterministic reflections at flat surfaces which are correlated due to the room geometry. The violation of the US assumption does not change the formulated bound or range estimators, but it will be important for future algorithm development if knowledge about these deterministic reflections is needed.

B. Evaluation and Comparison to Simulated Data

To be able to apply the ML and MF estimators to the acquired measurement data, we use the pre-processing steps laid out in Sec. III-C to derive the CRs at the target bandwidth, and add AWGN (generated with the previously defined N_0)

[3]The estimation of the covariance matrix as described here is for the validation of the REB only. It is not a practical algorithm to be used in actual ranging / positioning applications.

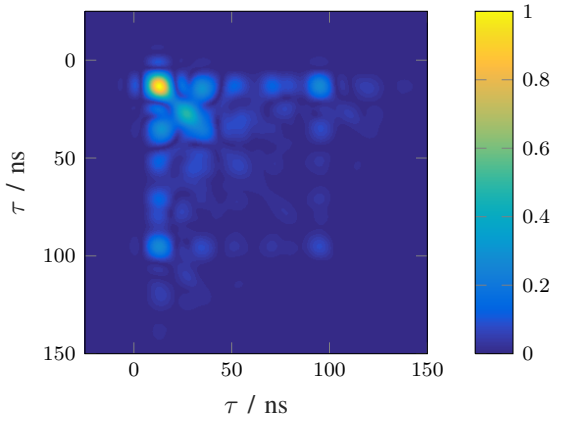

Fig. 4. Estimated covariance matrix of dense multipath at $B = 100\,\text{MHz}$ for the backscatter channel from antenna 1 via tag 1 to antenna 1 measured in the laboratory scenario.

to obtain the received signal described in (5). For comparison, simulated data are generated, by setting the parameters of the individual channels in such a way that the overall BS channel's parameters (K_{LOS} and τ_{rms}) match the measured data.

In Fig. 5, the SINR, effective SINR $\widetilde{\text{SINR}}_{\text{BS}}$, whitening gain γ and information loss $\sin^2(\varphi)$ are shown for different bandwidths for both scenarios (solid lines). The SINR tends towards the SNR and towards the K_{LOS} factor for large and small bandwidth respectively. In comparison, the effective SINR is achieving the SNR also at small bandwidth. The SINR and $\widetilde{\text{SINR}}_{\text{BS}}$ describe the amplitude fading and the pulse distortion of the LOS component respectively. At very large bandwidth neither pulse distortion nor amplitude fading occur as the DM is resolved from the LOS component. At small bandwidth only "flat" amplitude fading occurs as the complete DM overlaps with the LOS component. In-between these two extreme cases, both effects occur and deteriorate the ranging precision which is described by $\widetilde{\text{SINR}}_{\text{BS}}$. The two factors linking the SINR and $\widetilde{\text{SINR}}_{\text{BS}}$ are the whitening gain $\gamma \geq 1$ and the information loss $\sin^2(\varphi) \leq 1$. In both scenarios, the comparison to simulated data (dashed lines) shows an excellent match over the entire considered bandwidth range. The main difference is the negative whitening gain at large bandwidths in Fig. 5a which is explained by a frequency dependent behavior of the antenna pattern. The useful bandwidth in this case is actually smaller than 1 GHz explaining the negative whitening gain. As the bandwidth gets smaller, the frequency dependent behavior vanishes and the simulated data fits the actual measurements. In Scenario B, this effect is not visible due to the different geometric setup.

In Fig. 6, the ranging error bound and the standard deviations of the two introduced estimators are shown for a SISO ranging scenario. The MF estimator (circles) deviates from the performance bound already at large BW due to early reflections by the surroundings. The ML estimator on the other hand is able to achieve the bound down to a bandwidth in the region of 100 MHz where it achieves a precision

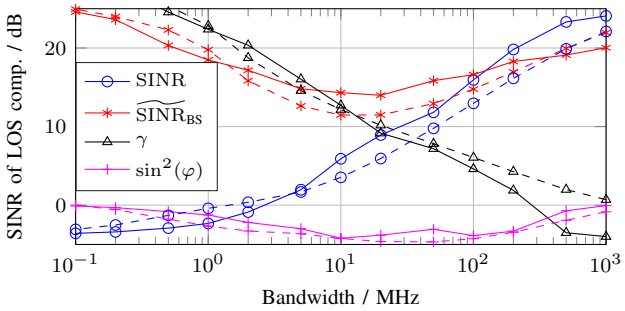

(a) Scenario A: measured data (solid lines / TX antenna at $\mathbf{p}_1$, table position T2, RX antenna at $\mathbf{p}_2$ / $K_{\text{LOS}} = -3\,\text{dB}$, $\tau_{\text{rms}} = 18.3\,\text{ns}$) and simulated data (dashed lines / the PDP of the downlink and uplink have been modeled with a double exp. PDP [4] with the following parameters: $K_{\text{LOS},\ell} = 1.3\,\text{dB}$, $\chi = 0.98$, $\gamma_r = 3.5\,\text{ns}$, $\gamma_d = 14\,\text{ns}$. The sim. BS channel thus has the following parameters: $K_{\text{LOS}} = -3\,\text{dB}$, $\tau_{\text{rms}} = 18.6\,\text{ns}$).

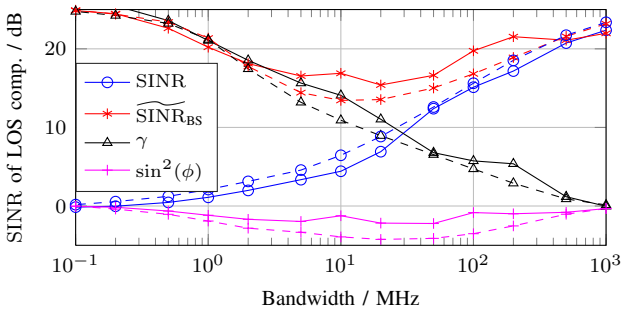

(b) Scenario B: measured data (solid lines / TX antenna at $\mathbf{p}_2$, table position T3, RX antenna at $\mathbf{p}_4$ / $K_{\text{LOS}} = 0.22\,\text{dB}$, $\tau_{\text{rms}} = 18.2\,\text{ns}$) and simulated data (dashed lines / the PDP of the downlink and uplink have been modeled with a double exp. PDP [4] with the following parameters: $K_{\text{LOS},\ell} = 3.9\,\text{dB}$, $\chi = 0.98$, $\gamma_r = 4.25\,\text{ns}$, $\gamma_d = 17\,\text{ns}$. The sim. BS channel thus has the following parameters: $K_{\text{LOS}} = 0.2\,\text{dB}$, $\tau_{\text{rms}} = 18.4\,\text{ns}$).

Fig. 5. SINR, $\widetilde{\text{SINR}}_{\text{BS}}$, whitening gain γ, and information loss $\sin^2(\varphi)$ for measured (solid lines) and simulated data (dashed lines).

below 20 cm. Below this bandwidth, a robust detection of the LOS component cannot be achieved since the SINR, which quantifies the SNR after the whitening operation, falls below the detection threshold of about 12 dB. The MF estimator gets more robust here, especially for the measurements performed in the industrial hall. This is because the MF estimator makes use of the DM, when the small bandwidth causes the DM to arrive simultaneously with the LOS.

The precision can be increased by non-coherent combining of K closely-spaced measurements [11], leading to a $\sqrt{K}$-fold gain of the precision. This gain is shown in Fig. 6 for 4x4 and 2x2 MIMO setups leading to a ranging precision better than 10 cm at a bandwidth of 100 MHz. A second advantage of diversity combining is a detection gain which makes it possible to follow the bound to smaller bandwidths due to a K-fold increase in SINR.

In Table I an overview of the achievable ranging precision is listed for three different operating scenarios (SISO, 2x2 MIMO & 4x4 MIMO) at three different bandwidths. The bandwidths are chosen to fit into the ETSI and FCC regulations and the 2.4 GHz ISM band. For a SISO operating scenario the ranging precision is 6.4, 0.84, and 0.2 m in the ETSI, the FCC and the

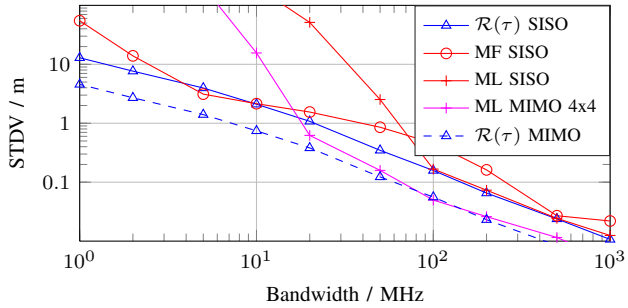

(a) Scenario A: Channel parameters see Fig. 5a.

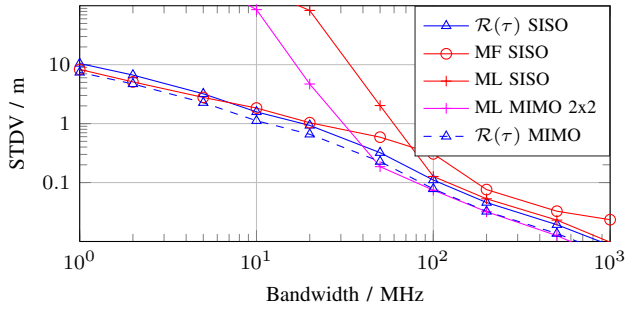

(b) Scenario B: Channel parameters see Fig. 5b

Fig. 6. Ranging error bound and range estimation standard deviations. Solid lines present measured data, the dashed line is the simulated REB with the according channel parameters.

Table I: Summary of the achievable ranging error bounds for three different operating scenarios (SISO, 2x2 MIMO & 4x4 MIMO) at three different bandwidths (according to the regulations of the ETSI (EU), FCC (US) and for operation in the 2.4 GHz ISM band). The REB has been simulated with the channel parameters given in Fig. 5b.

	Bandwidth		
	ETSI 3 MHz	FCC 26 MHz	ISM 83.5 MHz
REB SISO in m	6.4	0.84	0.20
REB MIMO 2x2 in m	3.2	0.42	0.10
REB MIMO 4x4 in m	1.6	0.21	0.05

ISM band, respectively.

VI. Conclusions

In this paper we analyzed channel measurements in the UHF-RFID frequency band, obtained in two different environments, a laboratory and an industrial hall. Wideband channel parameters have been analyzed, e.g. the Rician K-factor for the LOS component and the rms delay spread. These parameters influence the achievable ranging performance which can be quantified with a Cramér Rao lower bound. This bound on the ranging error standard deviation has been validated with two different estimators, a maximum likelihood and a matched filter estimator. The theoretical ranging precision is below 20 cm for a SISO system and below 10 cm for a MIMO system at a bandwidth of 100 MHz. Future research will focus on the main limitation of the current approach, namely the need to know the statistics of the dense multipath.

References

[1] J. D. Griffin and G. D. Durgin, "Gains for RF tags using multiple antennas," *IEEE Trans. Antennas Propag.*, vol. 56, no. 2, pp. 563–570, Feb 2008.

[2] D. Arnitz, U. Muehlmann, and K. Witrisal, "Wideband characterization of backscatter channels: Derivations and theoretical background," *IEEE Trans. Antennas Propag.*, vol. 60, no. 1, pp. 257–266, Jan 2012.

[3] M. S. Varela and M. G. Sanchez, "RMS delay and coherence bandwidth measurements in indoor radio channels in the UHF band," *IEEE Trans. Veh. Technol.*, vol. 50, no. 2, pp. 515–525, Mar 2001.

[4] J. Karedal, S. Wyne, P. Almers, F. Tufvesson, and A. F. Molisch, "A measurement-based statistical model for industrial ultra-wideband channels," *IEEE Trans. Wireless Commun.*, vol. 6, no. 8, pp. 3028–3037, August 2007.

[5] A. G. Dimitriou, S. Siachalou, A. Bletsas, and J. N. Sahalos, "A site-specific stochastic propagation model for passive UHF RFID," *IEEE Antennas Wireless Propag. Lett.*, vol. 13, pp. 623–626, 2014.

[6] H. Arthaber, T. Faseth, and F. Galler, "Spread-spectrum based ranging of passive UHF EPC RFID tags," *IEEE Commun. Lett.*, vol. 19, no. 10, pp. 1734–1737, Oct 2015.

[7] D. Dardari, R. D'Errico, C. Roblin, A. Sibille, and M. Z. Win, "Ultra-wide bandwidth RFID: The next generation?" *Proc. IEEE*, vol. 98, no. 9, pp. 1570–1582, Sept 2010.

[8] S. Hinteregger, E. Leitinger, P. Meissner, and K. Witrisal, "MIMO gain and bandwidth scaling for RFID positioning in dense multipath channels," in *IEEE International Conference on RFID*, May 2016.

[9] Y. Shen and M. Z. Win, "Fundamental limits of wideband localization-part i: A general framework," *IEEE Trans. Inf. Theory*, vol. 56, no. 10, pp. 4956–4980, 2010.

[10] D. Dardari, A. Conti, U. Ferner, A. Giorgetti, and M. Z. Win, "Ranging with ultrawide bandwidth signals in multipath environments," *Proc. IEEE*, vol. 97, no. 2, pp. 404–426, 2009.

[11] K. Witrisal, E. Leitinger, S. Hinteregger, and P. Meissner, "Bandwidth scaling and diversity gain for ranging and positioning in dense multipath channels," *IEEE Wireless Communications Letters*, vol. 5, no. 4, pp. 396–399, Aug 2016.

[12] D. Arnitz, U. Muehlmann, T. Gigl, and K. Witrisal, "Wideband system-level simulator for passive UHF RFID," in *2009 IEEE International Conference on RFID*, April 2009, pp. 28–33.

[13] C. Floerkemeier and S. Sarma, "RFIDSim - a physical and logical layer simulation engine for passive RFID," *IEEE Trans. Autom. Sci. Eng.*, vol. 6, no. 1, pp. 33–43, Jan 2009.

[14] B. Qi and F. Shen, "Propagation models for multi-hop wireless networks in ns-2 simulator," in *2011 Eighth International Conference on Information Technology: New Generations*, April 2011, pp. 701–706.

[15] A. F. Molisch, *Wireless Communications*. Wiley-IEEE Press, 2005.

[16] ——, "Ultra-wide-band propagation channels," *Proc. IEEE*, vol. 97, no. 2, pp. 353–371, Feb 2009.

[17] P. V. Nikitin, K. V. S. Rao, and R. D. Martinez, "Differential RCS of RFID tag," *Electronics Letters*, vol. 43, no. 8, pp. 431–432, 04 2007.

[18] F. Guidi, "Study of ultra wide band modulated backscattering based RFID systems," Ph.D. dissertation, Ecole Polytechnique Paristech, Universita degli studi di Bologna, 2013.

[19] S. Kay, *Fundamentals of Statistical Signal Processing: Estimation Theory*. Prentice Hall Signal Processing Series, 1993.

[20] Ilmsens Channel Sounder. [Online]. Available: http://www.ilmsens.com

[21] Mini Circuits, RC-4SPDT-A18 and RC-1SP4T-A18. [Online]. Available: http://www.minicircuits.com

[22] S. Hinteregger, E. Leitinger, P. Meissner, J. Kulmer, and K. Witrisal, "Bandwidth dependence of the ranging error variance in dense multipath," in *2016 24th European Signal Processing Conference (EUSIPCO) (EUSIPCO 2016)*, Budapest, Hungary, Aug. 2016.